

**Transient field  $g$  factor and mean-life measurements with a rare isotope beam of  $^{126}\text{Sn}$** G. J. Kumbartzki,<sup>\*</sup> N. Benczer-Koller, D. A. Torres,<sup>†</sup> B. Manning, P. D. O'Malley, Y. Y. Sharon, and L. Zamick  
*Department of Physics and Astronomy, Rutgers University, New Brunswick, New Jersey 08903, USA*C. J. Gross and D. C. Radford  
*Physics Division, Oak Ridge National Laboratory, Oak Ridge, Tennessee 37831, USA*S. J. Q. Robinson  
*Department of Physics, Millsaps College, Jackson, Mississippi 39210, USA*J. M. Allmond  
*Joint Institute for Heavy Ion Research, Oak Ridge National Laboratory, Oak Ridge, Tennessee 37831, USA*A. E. Stuchbery  
*Department of Nuclear Physics, Australian National University, Canberra, ACT 0200, Australia*K.-H. Speidel  
*Helmholtz-Institut für Strahlen- und Kernphysik, Universität Bonn, Bonn, Germany*N. J. Stone<sup>‡</sup> and C. R. Bingham  
*Department of Physics and Astronomy, University of Tennessee, Knoxville, Tennessee 37996, USA*  
(Received 31 July 2012; published 14 September 2012)**Background:** The  $g$  factors and lifetimes of the  $2_1^+$  states in the stable, proton-rich Sn isotopes have been measured, but there is scant information on neutron-rich Sn isotopes.**Purpose:** Measurement of the  $g$  factor and the lifetime of the  $2_1^+$  state at 1.141 MeV in neutron-rich  $^{126}\text{Sn}$  ( $T_{1/2} = 2.3 \times 10^5$  y).**Method:** Coulomb excitation in inverse kinematics together with the transient field and the Doppler shift attenuation techniques were applied to a radioactive beam of  $^{126}\text{Sn}$  at the Holifield Radioactive Ion Beam Facility.**Results:**  $g(2_1^+) = -0.25(21)$  and  $\tau(2_1^+) = 1.5(2)$  ps were obtained.**Conclusions:** The data are compared to large-scale shell-model and quasiparticle random-phase calculations. Neutrons in the  $h_{11/2}$  and  $d_{3/2}$  orbitals play an important role in the structure of the  $2_1^+$  state of  $^{126}\text{Sn}$ . Challenges, limitations, and implications for such experiments at future rare isotope beam facilities are discussed.DOI: [10.1103/PhysRevC.86.034319](https://doi.org/10.1103/PhysRevC.86.034319)

PACS number(s): 21.10.Ky, 25.70.De, 27.60.+j, 21.10.Tg

**I. INTRODUCTION**

The Sn isotopes, with the magic proton number  $Z = 50$ , provide a remarkably long chain of nuclei with neutrons filling gradually the whole range between the magic numbers  $N = 50$  and  $N = 82$ . Among the even- $A$  Sn nuclei,  $^{112-124}\text{Sn}$  are stable. The other even- $A$  Sn isotopes are radioactive and a few of them have only recently become available as rare isotope beams and accessible for nuclear spectroscopy.

A variety of techniques has been used to study the Sn nuclei. These include mass and two-neutron separation-energy measurements [1], pick-up and stripping reactions to determine single-particle energy levels [2,3], Coulomb-excitation and lifetime measurements to obtain quadrupole moments and transition probabilities, and magnetic-moment

measurements which help establish the specific neutron and proton contributions to the wave functions of the states of interest [4–8]. The resulting large and often precise body of experimental evidence has established the basic structure of the Sn isotopes against which theoretical calculations, using different approaches and interactions, can be tested. The  $B(E2; 2_1^+ \rightarrow 0_1^+)$  values have been measured from  $^{106}\text{Sn}$  to  $^{134}\text{Sn}$  ([6,8] and references therein). The current status of the  $g$  factors of the  $2_1^+$  states in the even- $A$  Sn isotopes is summarized in Fig. 1. These measurements by East *et al.* [5], Walker *et al.* [7], and Hass *et al.* [9] all used the transient field technique. Preliminary results for the absolute  $g$ -factor values of the  $2_1^+$  states in  $^{124}\text{Sn}$  and  $^{126}\text{Sn}$ , measured by the recoil-in-vacuum technique (RIV), were reported at a meeting at Hilton Head in 2011 [10].

The general trend of the measured magnetic moments in the stable Sn isotopes shown in Fig. 1 runs from positive values for the lighter isotopes to negative values for the heavier nuclei. But the magnitude and even the sign of some magnetic moments are not reproduced in separate experiments. As these

<sup>\*</sup>kum@physics.rutgers.edu<sup>†</sup>Current Address: Departamento de Física, Universidad Nacional de Colombia, Carrera 30 No. 45-03, Bogotá D.C., Colombia.<sup>‡</sup>Department of Physics, Oxford University, OX1 3PU Oxford, UK.

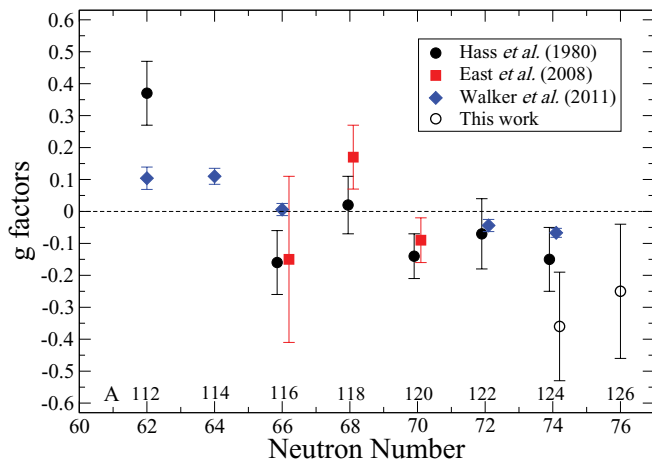


FIG. 1. (Color online) The  $g$  factors of the  $2_1^+$  states for even- $A$  Sn isotopes.

$g$  factors are crucial elements in the determination of the occupation of shell-model orbitals by neutrons and protons, the current experiment on  $^{126}\text{Sn}$  was undertaken to determine its  $g(2_1^+)$  factor, including its sign, and to extend the transient field technique to radioactive neutron-rich Sn nuclei. The same data were used to determine the lifetime of the  $2_1^+$  state. Values for the  $g$  factor and lifetime of the  $2_1^+$  state in  $^{124}\text{Sn}$  were obtained as a by-product of the tuning of the accelerator for the radioactive  $^{126}\text{Sn}$  beam experiment.

## II. THE EXPERIMENT

Transient field experiments involving Coulomb excitation of a heavy beam in inverse kinematics by the first (light) element of a multilayered ferromagnetic target have been used for many years [11,12]. The technique has been successfully extended to beams of radioactive isotopes such as  $^{76}\text{Kr}$  [13] and  $^{132}\text{Te}$  [14] to measure their  $g(2_1^+)$  factors. Complementary magnetic moment studies using radioactive beams have been carried out by the RIV technique on  $^{132}\text{Te}$  [15] and  $^{126}\text{Sn}$  [10].

In a typical stable-beam experiment all the particles are stopped in the target chamber: the excited projectile probe ions in the last layer of the target and the beam either in the target or in an extra stopper foil behind the target. Both the target and the stopper foil are thin enough so that the light knock-on particles from the first target layer can reach a particle detector, which is mounted at zero degrees with respect to the beam direction.

The work with radioactive projectiles requires modifications to the experimental setup to minimize radioactivity buildup in and near the target. The details of the modifications depend largely on the half-life of the radioactive species, on the isobaric contamination, and on the beam profile. The earlier experiments, Refs. [13,14], provide different ways of dealing with the accumulating radioactivity. While in one experiment the beam was stopped in a moving tape located behind the target, the beam and most of the activity in the other experiment were stopped in a distant beam dump.

In the present experiment  $^{126}\text{Sn}$  has such a long half-life ( $T_{1/2} = 2.3 \times 10^5 \text{y}$ ) that it could be considered “stable.”

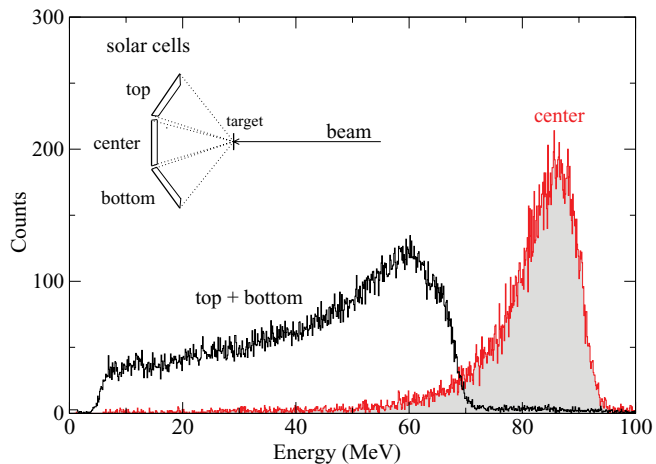


FIG. 2. (Color online) Spectra observed in the central and adjoining solar cells.

Therefore, this experiment was approached like a stable-beam experiment, although some isobaric beam contamination had to be expected. The exact level of the beam contamination and its effect on the overall counting rate were initially unknown. The contaminant  $^{126}\text{Sb}$  ( $T_{1/2} = 19.15 \text{min}$ ) decays to  $^{126}\text{Te}$ . Nevertheless, it was decided to stop the beam in the target chamber, but not in the target itself. The beam was stopped in an additional catcher foil, mounted behind the target and designed to be replaced should the counting rate in the  $\gamma$  detectors become too high. As it turned out, this concern was unfounded.

The  $^{126}\text{Sn}$  beams were prepared at the Holifield Radioactive Beam Facility by the ORIC/U fission source/Tandem systems [16] at Oak Ridge National Laboratory from an initial bombardment of a uranium target by 50 MeV protons. The activity was incorporated into SnS molecules. Since the Sb and Te isobars do not easily form sulfides, their contamination in the  $^{126}\text{Sn}$  beam is reduced by 4–5 orders of magnitude.

The multilayered target consisted (front to back) of 1.0 mg/cm<sup>2</sup> carbon, 5.01 mg/cm<sup>2</sup> gadolinium, 1.1 mg/cm<sup>2</sup> tantalum, and 5.04 mg/cm<sup>2</sup> copper. At the beam energy of 378 MeV the inelastically scattered  $^{126}\text{Sn}$  ions exited the target with less than 5 MeV and were stopped, together with the beam, in the 5.6 mg/cm<sup>2</sup> copper foil mounted at the back of the target frame. The forward-scattered C ions were detected in an array of three solar cells, each 15 × 15 mm, mounted vertically 30 mm downstream of the target. The center cell was placed at zero degrees with respect to the beam axis and covered an opening angle of  $\pm 14^\circ$ . The two other cells were mounted above and below the center cell as shown in Fig. 2. The vertical opening angle of the detector array was  $\pm 46^\circ$ . The solar cells were covered by 5.6 mg/cm<sup>2</sup> copper. In this arrangement the useful opening angle for detecting C ions was kinematically limited to  $\pm 38^\circ$ . Above this angle the C-ion energy was below the  $\sim 4 \text{MeV}$  detection cutoff. The target was held between the pole pieces of an electromagnet which provided a magnetic field of 0.07 T, large enough to saturate the gadolinium layer of the target. The whole magnet assembly, inside the vacuum chamber, was cooled by liquid nitrogen to  $\sim 77 \text{K}$ . The magnetization of the target was measured

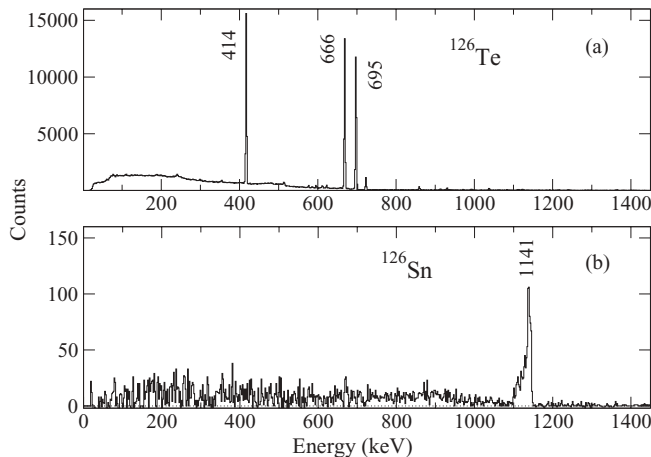


FIG. 3. (a) Singles  $\gamma$ -ray spectrum in one clover segment showing the transitions in  $^{126}\text{Te}$  arising from the decay of the contaminant  $^{126}\text{Sb}$  in the beam. (b) All the  $\gamma$  rays in coincidence with particles selected in all solar cells for both backward clover detectors. The randoms subtraction eliminated effectively all  $\gamma$  lines stemming from the radioactive beam contamination.

off-line in an ac magnetometer and was found to be constant at  $M = 0.18$  T between 50 K and 120 K.

The  $\gamma$  radiation was detected in four clover Ge detectors mounted at a distance of 120 mm from the target: two at backward angles ( $\pm 113^\circ$ ) and two at forward angles ( $\pm 67^\circ$ ). The energy and time information of every singles event in each detector segment was determined directly from the preamplifier signals in digitizing PIXIE-4 pulse processors from XIA [17] and stored on disk. The magnetic field direction was switched from the up to the down position every 90 sec and was recorded with every particle.

The particle spectra obtained in the central detector and in the adjoining upper and lower detectors are shown in Fig. 2. The spectra of  $\gamma$  rays, as singles and in coincidence with the particles, are shown in Fig. 3. The singles spectrum shown is for one clover segment taken over a period of 36 min at 16 hours into the radioactive beam run. Although the  $\gamma$  singles spectra are dominated by lines from the decay of radioactive  $^{126}\text{Sb}$ , their intensity never overwhelmed the germanium detectors. The  $\gamma$  singles rate was usually  $\lesssim 500$  cps in each clover segment. Therefore, it was not necessary to change the catcher foil behind the target throughout the experiment.

The experiment was carried out at a beam energy of 378 MeV which is about 20% below the Coulomb barrier for  $^{126}\text{Sn}$  on  $^{12}\text{C}$ . The average beam intensity was  $(1-3) \times 10^6$  pps as measured in a Faraday cup and a microchannel plate detector. In total, 135 hours of radioactive  $^{126}\text{Sn}$  beam were run. Altogether a total of about 1750 coincident counts were collected in the full energy peaks of all detectors, which amounts to  $\sim 13$  counts per hour.

### III. LIFETIME MEASUREMENTS

The lifetimes of the  $2_1^+$  states in the  $^{124}\text{Sn}$  and  $^{126}\text{Sn}$  nuclei were determined from the line shapes of the  $\gamma$  transitions

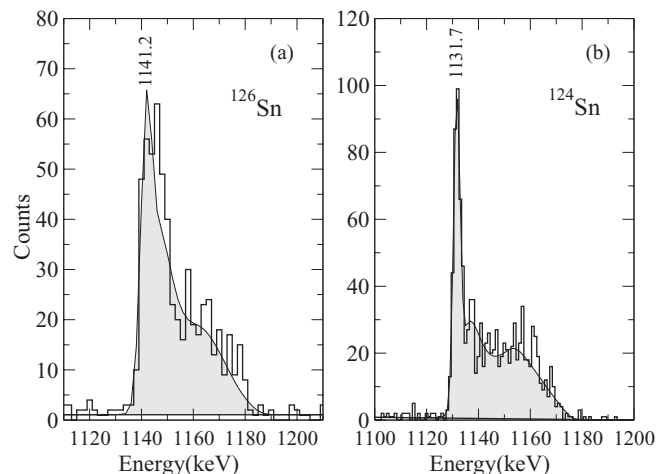


FIG. 4. Line-shape fits of the  $(2_1^+ \rightarrow 0_1^+)$  transition in  $^{126}\text{Sn}$  (a) and  $^{124}\text{Sn}$  (b) at a detector angle of  $59^\circ$ . The broad stopped peak in  $^{126}\text{Sn}$  is due to decay in a gap between the multilayer target and attached stopper foil (see text).

observed in pairs of clover detector elements located at the same angle. Only the most forward and backward clover segments were used. For  $^{126}\text{Sn}$  all spectra were carefully gain matched and added together for the fit. The LINESHAPE code [18] was used as described in a previous publication [19]. The line-shape analysis took into account the fact that the ions were not stopped in the target but in an extra foil located close behind the target. The ion velocity in the 0.1–0.3 mm gap between the target and the foil was about  $0.01c$ . The decays in the gap add intensity to the tail near the stopped peak energy. This part of the spectrum was treated as a “contaminant peak” (Doppler broadened, fully shifted) in the fitting procedure. The final quoted lifetime is an averaged result from independent fits of data from segments of all four clover detectors. In Fig. 4(a) the corresponding calculated line shape together with the data of the forward detectors at  $59^\circ$  for  $^{126}\text{Sn}$  is presented.

The  $^{124}\text{Sn}$  lifetime data were taken under the preliminary setup conditions before the  $^{126}\text{Sn}$  beam was obtained. The data shown in Fig. 4(b) were taken at a beam energy of 372 MeV and with a different target ( $0.61$  C/ $6.46$  Gd/ $1.0$  Ta/ $5.6$  Cu mg/cm $^2$ ) at room temperature. In this case the  $^{124}\text{Sn}$  ions stopped in the target.

### IV. MAGNETIC MOMENT MEASUREMENT

The magnetic moment of a given state is determined from the measurement of the precession of this moment in the hyperfine field while the ions traverse the ferromagnetic foil. The precession gives rise to a rotation of the particle- $\gamma$  angular correlation. This rotation is obtained from the change in the intensity of the particle- $\gamma$  coincidence rate as the direction of the magnetic field at the target is changed from up to down with respect to the plane defined by the  $\gamma$  detectors. The precession angle,  $\Delta\theta$ , is derived from counting rate ratios  $(N \uparrow - N \downarrow)/(N \uparrow + N \downarrow)$ , where  $N \uparrow \downarrow$  is the full energy peak intensity for the two field directions in each detector. As fully described in Ref. [12] double ratios can be calculated for

TABLE I. Summary of the kinematic parameters for the transient field measurement. The  $\langle E \rangle_{\text{in}}$  and  $\langle E \rangle_{\text{out}}$ , and  $\langle v/v_0 \rangle_{\text{in}}$  and  $\langle v/v_0 \rangle_{\text{out}}$ , are, respectively, the average energies and velocities of the excited  $^{126}\text{Sn}$  ions as they enter into, and exit from, the gadolinium layer;  $v_0 = e^2/\hbar$  is the Bohr velocity. Here  $T_{\text{eff}}$  is the effective transit time of the ions through the ferromagnetic layer. The  $\Delta\theta_{\text{calc}}$  is the expected precession angle of the magnetic moment for the target and kinematic conditions of this experiment, for  $g = 1$ , using the Rutgers parametrization [20].

Particle acceptance	$\langle E \rangle_{\text{in}}$ (MeV)	$\langle E \rangle_{\text{out}}$ (MeV)	$\langle v/v_0 \rangle_{\text{in}}$	$\langle v/v_0 \rangle_{\text{out}}$	$T_{\text{eff}}$ (fs)	$\Delta\theta_{\text{calc}}$ (mrad)
$0^\circ\text{--}14^\circ$	198	84	8.0	5.2	363	51(4)
$18^\circ\text{--}38^\circ$	226	103	8.5	5.7	340	50(4)

detector combinations which show the full rotation effect  $\epsilon$  or  $\epsilon_c$  for detector combinations where the rotation effect is canceled out. In the absence of systematic errors the so-called cross ratio  $\epsilon_c$  should be zero.

The kinematic parameters relevant to this experiment are compiled in Table I. The results of the precession measurement are given in Table II.

In experiments with radioactive beams an independent determination of the particle- $\gamma$  angular correlation is too time consuming. Therefore, the slope,  $S$ , of the angular correlation was determined, as in other experiments, from the precession data by making use of the multiple angles of individual clover segments [14].

## V. RESULTS

In this experiment the slopes derived from the data of the central and the peripheral particle detectors were, within their errors, the same. Therefore, the data sets of all particle detectors were combined for the precession analysis.

The measured slopes are typical for this type of reaction and detection geometry. Any attenuation of the correlation due to recoiling out of the target is negligible. The total precession angle,  $\Delta\theta = \epsilon/S$ , for the  $(2_1^+ \rightarrow 0_1^+)$  transition in  $^{126}\text{Sn}$  was  $\Delta\theta = 12.3(108)$  mrad, which yields  $g(^{126}\text{Sn}; 2_1^+) = -0.25(21)$ . The large error is dominated by the small number of counts in the full energy peak, and is a direct consequence of the low beam intensity and given running time. As a by-product, in short runs (totaling  $\sim 5$  hr) with a stable  $^{124}\text{Sn}$  beam, a value of  $g(^{124}\text{Sn}; 2_1^+) = -0.36(17)$  was obtained which is more negative than the value of  $g(2_1^+) = -0.067(14)$  reported in Ref. [7]. The observed large precession effect together with a near zero cross ratio support the current result.

TABLE II. Experimental and calculated  $g$  factors of the  $2_1^+$  states in the  $^{124,126}\text{Sn}$  isotopes. The  $\epsilon$ 's and  $\epsilon_c$ 's (see text) are double ratios of the measured counting rates in the full-energy  $\gamma$  peaks. Also included are the slopes and precession angles.

Isotope	$\epsilon$	$\epsilon_c$	$ S(67^\circ) $ (mrad $^{-1}$ )	$\Delta\theta$ (mrad)	$g$	
					Exp.	LSSM <sub>this work</sub>
$^{124}\text{Sn}$	0.038(18)	0.003(18)	2.16(10)	17.8(85)	-0.36(17)	-0.18
$^{126}\text{Sn}$	0.026(23)	0.002(23)	2.13(9)	12.3(108)	-0.25(21)	-0.18

The lifetime results are summarized in Table III. The line-shape fits provide a direct determination of the lifetime complementary to the lifetime obtained from  $B(E2)$  measurements [8]. For the  $2_1^+$  state in  $^{126}\text{Sn}$  a lifetime of  $\tau(^{126}\text{Sn}; 2_1^+) = 1.5(2)$  ps was obtained. The fit error was enlarged to take into account the uncertainty in modeling the recoil out of the target. The quoted error includes the spread in the fits to the data from all used detectors. Systematic error contributions due to questions about the stopping powers used in the calculation of the line shape are harder to estimate and were not included, but could potentially increase the uncertainty of the lifetime. The result is in agreement with the  $B(E2)$  value of Ref. [8]. For the calculation of  $\Delta\theta(g=1)$  an average of the measured and derived [from the  $B(E2)$  measurement] lifetimes,  $\tau = 1.6$  ps, was used.

The lifetime of the  $2_1^+$  state in  $^{124}\text{Sn}$  was also determined. Its value  $\tau(^{124}\text{Sn}; 2_1^+) = 1.58(10)$  ps is in agreement with the value of 1.48(15) ps reported in Ref. [6]. In the current experiment the  $2_1^+ \rightarrow 0_1^+$  transition is a well-resolved  $\gamma$  line with a better defined shape due to the larger recoil velocity available in inverse kinematics experiments.

## VI. THEORY

The structure of the low-lying states in the long chain of Sn isotopes between the  $^{100}\text{Sn}$  and  $^{132}\text{Sn}$  doubly closed shells has been extensively examined within the framework of several models. A compilation of theoretical values for  $^{126}\text{Sn}$  is presented in Fig. 5. The corresponding values for  $^{124}\text{Sn}$  are also included for comparison.

Two general approaches have been pursued, one based on the nonrelativistic [22–24] and relativistic [25–27] quasiparticle random phase approximation (QRPA) and the other on large-scale shell-model (LSSM) calculations [6,7,28,29].

### A. Quasiparticle random phase approximation calculations

The relativistic RQRPA [26] calculations qualitatively agree with the experimental excitation energies and  $B(E2)$  values for the whole region of Sn nuclei from the lightest to the heaviest.

The more recent calculations [24] carried out within the quasiparticle phonon model, with quadrupole pairing and with effective charges  $e_\pi = 1.05e$  and  $e_\nu = 0.05e$ , also reproduce the trend in the transition probabilities for the light Sn nuclei.

The experimental static quadrupole moments show that the unstable neutron-rich  $^{126,128}\text{Sn}$  nuclei have a deformation consistent with zero [8] as predicted by [22]. Actually, for

TABLE III. Summary of  $B(E2; 0_1^+ \rightarrow 2_1^+)$  values and lifetimes for the  $2_1^+$  states in the  $^{124,126}\text{Sn}$  isotopes. The  $B(E2)$ 's in this work and Ref. [6] were derived from the measured  $\tau$ . In Ref. [8] the  $B(E2)$ 's were measured recently by Coulomb excitation. The calculated values were obtained with  $e_v = 0.8e$ .

Isotope	$\tau$ (ps)		$B(E2)_{\text{exp}}$ ( $e^2b^2$ )			$B(E2)_{\text{calc}}$ ( $e^2b^2$ )
	This work	Ref. [6]	This work	Ref. [6]	Ref. [8]	LSSM <sub>this work</sub>
$^{124}\text{Sn}$	1.58(10)	1.48(15)	0.140(10)	0.148(15)	0.162(6) <sup>a</sup>	0.148
$^{126}\text{Sn}$	1.50(20)		0.140(20)		0.127(8)	0.117

<sup>a</sup>In agreement with  $B(E2; 0_1^+ \rightarrow 2_1^+) = 0.166(4) e^2b^2$  of the compilation in Ref. [21].

$^{126}\text{Sn}$ , in a pure six-particle/six-hole  $h_{11/2}$  configuration, the shell is half filled and the static quadrupole moment of the  $2_1^+$  state should be zero. The magnetic moments of the  $2_1^+$  states of the even-A Sn isotopes were calculated with the same tools as the  $B(E2)$  values [5,7,22,27,30].

The QRPA calculation [27] yields positive  $g$  values up to  $^{126}\text{Sn}$ , and a negative value at  $^{128}\text{Sn}$ , while the experimental values of the magnetic moment become negative around  $^{116}\text{Sn}$ . However, in Ref. [27] it is also shown that if only the neutron contribution is considered then all calculated  $g$  values are negative and reach a minimum at  $^{130}\text{Sn}$ .

Terasaki [22] calculated approximately constant negative values of the magnetic moments for the even-A  $^{116-126}\text{Sn}$  isotopes using a separable quadrupole plus pairing Hamiltonian and the nonrelativistic QRPA. The results of these calculations are in qualitative agreement with experiment. The most recent calculation by Stoyanov [30] within the quasiparticle phonon model (QPM) yields a value of  $g(^{126}\text{Sn}; 2_1^+) = -0.121$ .

## B. Large-scale shell-model calculations

In the present paper LSSM calculations were carried out for  $^{124,126}\text{Sn}$ . The calculations assumed a strictly closed  $Z = 50$  proton core and included the ( $d_{5/2}$ ,  $g_{7/2}$ ,  $s_{1/2}$ ,  $d_{3/2}$ , and  $h_{11/2}$ ) neutron orbitals outside a  $^{100}\text{Sn}$  core. The sn100pn interaction within the shell-model code Nushell [31] was used.

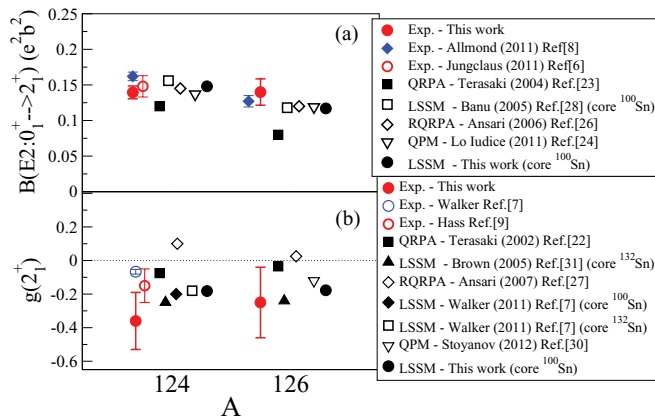


FIG. 5. (Color online) A compilation of calculated  $B(E2; 0_1^+ \rightarrow 2_1^+)$  (a) and  $g(2_1^+)$  (b) values including the experimental data (points with error bars) for  $^{124}\text{Sn}$  and  $^{126}\text{Sn}$ . The core ( $^{100}\text{Sn}$  or  $^{132}\text{Sn}$ ) used in each LSSM calculation is indicated in the legend.

The subsequent discussion is simplified by considering holes instead of particles. Table IV shows the results of these calculations for the average occupation numbers of the single-particle orbitals by neutron holes in the  $0_1^+$  and  $2_1^+$  states in  $^{124,126}\text{Sn}$  (see also Ref. [7]). The  $h_{11/2}$  and  $d_{3/2}$  are the only orbitals with more than one hole both in  $^{124}\text{Sn}$  and  $^{126}\text{Sn}$ . Furthermore, in the three odd nuclei  $^{123,125,127}\text{Sn}$  the observed ground states are  $(11/2)^-$  while the low-lying first excited states are  $(3/2)^+$ . In a simple  $h_{11/2}$  and  $d_{3/2}$  neutron hole space picture for  $^{124,126}\text{Sn}$  positive-parity state configurations require even numbers of  $h_{11/2}$  or  $d_{3/2}$  holes. In that space, assuming all the other holes couple to zero, only two two-hole configurations can form a  $2^+$  state. One is the  $(h_{11/2})_v^2$  configuration whose Schmidt  $g$  factor is  $g(h_{11/2})_v = -0.35$ , in agreement within their errors with the  $g$  factors measured in the present experiment. The other configuration,  $(d_{3/2})_v^2$ , has a large positive  $g$  factor of  $g(d_{3/2})_v = +0.765$  which disagrees with the present experimental results. The above discussion suggests that neutron holes in the  $h_{11/2}$  orbital play a dominant role in the structure of the  $2_1^+$  states in  $^{124}\text{Sn}$  and  $^{126}\text{Sn}$ .

The LSSM wave functions are fractionated. A study of the  $2_1^+$  wave function in  $^{126}\text{Sn}$  shows that the largest configuration (26.3%) involves exciting two  $d_{3/2}$  neutrons into the  $h_{11/2}$  orbital. On the other hand, for the  $2_1^+$  state in  $^{124}\text{Sn}$  the two largest configurations involve exciting either two  $d_{3/2}$  neutrons into the  $h_{11/2}$  orbital (12.4%), or two  $s_{1/2}$  neutrons into the  $h_{11/2}$  orbital (11.2%).

The results of the LSSM calculations for excitation energies,  $E_x(^{124}\text{Sn}; 2_1^+) = 1.094$  MeV and  $E_x(^{126}\text{Sn}; 2_1^+) = 1.127$  MeV, are in good agreement with the experimental  $2_1^+$  energies, 1.132 MeV and 1.141 MeV, respectively.

The  $g$ -factor calculations for  $^{124,126}\text{Sn}$  using free-nucleon  $g$  factors yield the same value of  $g_{\text{calc}}(2_1^+) = -0.18$  for both isotopes (Table II). This value is close to the  $h_{11/2}$  empirical single-particle  $g$  factor of  $-0.25$  (Table VII in Ref. [7]). The experimental value of  $g(2_1^+; ^{126}\text{Sn}) = -0.25(21)$  with its

TABLE IV. Average occupation of neutron holes in single-particle orbits for the ground and the  $2_1^+$  states in  $^{124,126}\text{Sn}$  from large-scale shell-model calculations using a  $^{100}\text{Sn}$  core.

Isotope	$I^\pi$	$h_{11/2}$	$g_{7/2}$	$d_{5/2}$	$d_{3/2}$	$s_{1/2}$
$^{124}\text{Sn}$	$0_1^+$	4.11	0.68	0.69	1.78	0.54
	$2_1^+$	4.20	0.65	0.64	1.73	0.77
$^{126}\text{Sn}$	$0_1^+$	3.08	0.44	0.51	1.43	0.54
	$2_1^+$	3.16	0.38	0.45	1.44	0.57

large uncertainty cannot distinguish between the different theoretical predictions, but the larger negative  $g$ -factor values for both isotopes agree better with the trend of the LSSM results reported in Ref. [7].

The calculated  $B(E2; 2_1^+ \rightarrow 0_1^+)$  values depend on the the square of the effective charge  $e_\nu$  chosen for the neutron. The results shown in Table III were obtained with  $e_\nu = 0.8e$ . The large effective charge for the neutrons is required for the calculation in a pure neutron valence space to reproduce the experimental data and probably reflects the omission of proton excitations from the core.

## VII. SUMMARY

The  $g$  factor of the  $2_1^+$  state in  $^{126}\text{Sn}$  has been measured. Its sign has been determined as negative. The lifetimes of the first excited  $2_1^+$  states in  $^{124,126}\text{Sn}$  have been measured as well. Calculations of the reduced transition matrix elements within the framework of the QPM, QRPA, and RQRPA models are in agreement with the measurements. The LSSM

calculations of the  $E2$  reduced transition matrix elements using a neutron effective charge of  $e_\nu = 0.8e$  agree with the experimental data. The LSSM results show that neutron holes in the  $h_{11/2}$  and  $d_{3/2}$  orbitals play an important role in the structure of the  $^{126}\text{Sn}$   $2_1^+$  state. The experiment indicates the limitations of the transient field technique when used with low-intensity radioactive beams. Future experiments will need higher beam intensities and improved  $\gamma$  detection (larger solid angle coverage and increased detection efficiency) to yield more precise results.

## ACKNOWLEDGMENTS

The authors thank the staff of HRIBF who contributed to the smooth operation of the ORIC Cyclotron-Tandem accelerators and provided technical support. The authors also recognize the support of the US National Science Foundation (Rutgers group), of the Office of Nuclear Physics, US Department of Energy, and of the Australian Research Council, Grant No. DP0773273.

- 
- [1] G. Audi, O. Bersillon, J. Blachot, and A. H. Wapstra, *Nucl. Phys. A* **729**, 3 (2003).
- [2] J. P. Schiffer, S. J. Freeman, J. A. Caggiano, C. Deibel, A. Heinz, C.-L. Jiang, R. Lewis, A. Parikh, P. D. Parker, K. E. Rehm, S. Sinha, and J. S. Thomas, *Phys. Rev. Lett.* **92**, 162501 (2004).
- [3] K. L. Jones *et al.*, *Phys. Rev. C* **84**, 034601 (2011).
- [4] D. Radford *et al.*, *Nucl. Phys. A* **752**, 264 (2005).
- [5] M. East, A. Stuchbery, A. Wilson, P. Davidson, T. Kibédi, and A. Levon, *Phys. Lett. B* **665**, 147 (2008).
- [6] A. Jungclaus *et al.*, *Phys. Lett. B* **695**, 110 (2011).
- [7] J. Walker *et al.*, *Phys. Rev. C* **84**, 014319 (2011).
- [8] J. M. Allmond, D. C. Radford, C. Baktash, J. C. Batchelder, A. Galindo-Uribarri, C. J. Gross, P. A. Hausladen, K. Lagergren, Y. Larochele, E. Padilla-Rodal, and C.-H. Yu, *Phys. Rev. C* **84**, 061303 (2011).
- [9] M. Hass, C. Broude, Y. Niv, and A. Zemel, *Phys. Rev. C* **22**, 97 (1980).
- [10] J. M. Allmond, A. E. Stuchbery, D. C. Radford *et al.* (unpublished).
- [11] K.-H. Speidel, O. Kenn, and F. Nowacki, *Prog. Part. Nucl. Phys.* **49**, 91 (2002).
- [12] N. Benczer-Koller and G. J. Kumbartzki, *J. Phys. G: Nucl. Part. Phys.* **34**, R321 (2007).
- [13] G. Kumbartzki, J. R. Cooper, N. Benczer-Koller, K. Hiles, T. J. Mertzimekis, M. J. Taylor, K.-H. Speidel, P. Maier-Komor, L. Bernstein, M. A. McMahan, L. Phair, J. Powell, and D. Wutte, *Phys. Lett. B* **591**, 213 (2004).
- [14] N. Benczer-Koller, G. J. Kumbartzki, G. Gürdal, C. J. Gross, A. E. Stuchbery, B. Krieger, R. Hatarik, P. O'Malley, S. Pain, L. Segen, C. Baktash, J. Beene, D. C. Radford, C. Y. Yu, N. J. Stone, C. R. Bingham, M. Danchev, R. Grzywacz, and C. Mazzochi, *Phys. Lett. B* **664**, 241 (2008).
- [15] N. J. Stone, A. E. Stuchbery, M. Danchev, J. Pavan, C. L. Timlin, C. Baktash, C. Barton, J. R. Beene, N. Benczer-Koller, C. R. Bingham, J. Dupak, A. Galindo-Uribarri, C. J. Gross, G. Kumbartzki, D. C. Radford, J. R. Stone, and N. V. Zamfir, *Phys. Rev. Lett.* **94**, 192501 (2005).
- [16] J. R. Beene, D. W. Bardayan, A. G. Uribarri, C. J. Gross, K. L. Jones, J. F. Liang, W. Nazarewics, D. W. Stracener, B. A. Tatum, and R. L. Varner, *J. Phys. G: Nucl. Part. Phys.* **38**, 024002 (2011).
- [17] X-Ray Instrumentation Associates: <http://www.xia.com/>
- [18] J. C. Wells and N. R. Johnson, computer code LINESHAPE, 1999, PD-LNL version.
- [19] G. J. Kumbartzki, K.-H. Speidel, N. Benczer-Koller, D. A. Torres, Y. Y. Sharon, L. Zamick, S. J. Q. Robinson, P. Maier-Komor, T. Ahn, V. Anagnostatou, C. Bernards, M. Elvers, P. Goddard, A. Heinz, G. Ilie, D. Radeck, D. Savran, V. Werner, and E. Williams, *Phys. Rev. C* **85**, 044322 (2012).
- [20] N. K. B. Shu, D. Melnik, J. M. Brennan, W. Semmler, and N. Benczer-Koller, *Phys. Rev. C* **21**, 1828 (1980).
- [21] S. Raman, C. W. Nestor, Jr., and P. Tikkanen, *At. Data Nucl. Data Tables* **78**, 1 (2001).
- [22] J. Terasaki, J. Engel, W. Nazarewicz, and M. Stoitsov, *Phys. Rev. C* **66**, 054313 (2002).
- [23] J. Terasaki, *Nucl. Phys. A* **746**, 583 (2004).
- [24] N. Lo Iudice, C. Stoyanov, and D. Tarpanov, *Phys. Rev. C* **84**, 044314 (2011).
- [25] A. Ansari, *Phys. Lett. B* **623**, 37 (2005).
- [26] A. Ansari and P. Ring, *Phys. Rev. C* **74**, 054313 (2006).
- [27] A. Ansari and P. Ring, *Phys. Lett. B* **649**, 128 (2007).
- [28] A. Banu *et al.*, *Phys. Rev. C* **72**, 061305 (2005).
- [29] J. Cederkäll *et al.*, *Phys. Rev. Lett.* **98**, 172501 (2007).
- [30] C. Stoyanov (private communication).
- [31] B. A. Brown and W. D. Rae, computer code NushellsMSU, 2007, MSU-NSCL report.